
Numerical modeling of bedload and suspended load contributions to morphological evolution of the Seine Estuary (France)

Mengual Baptiste ^{1,2,*}, Le Hir Pierre ¹, Rivier Aurélie ^{1,3}, Caillaud Matthieu ¹, Grasso Florent ¹

¹ IFREMER, DYNECO/DHYSED Laboratory, Centre de Bretagne, CS 10070, 29280, Plouzané, France

² UMR 7266 LIENSs, CNRS-La Rochelle University, 17000, La Rochelle, France

³ IRSN (Institut de Radioprotection et de Sûreté Nucléaire), PRP-ENV/SERIS/LRC Laboratory, 50130, Cherbourg-Octeville, France

* Corresponding author : Baptiste Mengual, email address : bapt.mengual@hotmail.fr

Abstract :

This numerical modeling study (i) assesses the influence of the sediment erosion process on the sediment dynamics and subsequent morphological changes of a mixed-sediment environment, the macrotidal Seine estuary, when non-cohesive particles are dominant within bed mixtures (non-cohesive regime), and (ii) investigates respective contributions of bedload and suspended load in these dynamics. A three dimensional (3D) process-based morphodynamic model was set up and run under realistic forcings (including tide, waves, wind, and river discharge) during a 1-year period. Applying erosion homogeneously to bed sediment in the non-cohesive regime, i.e., average erosion parameters in the erosion law (especially the erodibility parameter, E_0), leads to higher resuspension of fine sediment due to the presence of coarser fractions within mixtures, compared to the case of an independent treatment of erosion for each sediment class. This results in more pronounced horizontal sediment flux (two-fold increase for sand, +30% for mud) and erosion/deposition patterns (up to a two-fold increase in erosion over shoals, generally associated with some coarsening of bed sediment). Compared to observed bathymetric changes, more relevant erosion/deposition patterns are derived from the model when independent resuspension fluxes are considered in the non-cohesive regime. These results suggest that this kind of approach may be more relevant when local grain-size distributions become heterogeneous and multimodal for non-cohesive particles. Bedload transport appears to be a non-dominant but significant contributor to the sediment dynamics of the Seine Estuary mouth. The residual bedload flux represents, on average, between 17 and 38% of the suspended sand flux, its contribution generally increasing when bed sediment becomes coarser (can become dominant at specific locations). The average orientation of residual fluxes and erosion/deposition patterns caused by bedload generally follow those resulting from suspended sediment dynamics. Sediment mass budgets cumulated over the simulated year reveal a relative contribution of bedload to total mass budgets around 25% over large erosion areas of shoals, which can even become higher in sedimentation zones. However, bedload-induced dynamics can locally differ from the dynamics related to suspended load, resulting in specific residual transport, erosion/deposition patterns, and changes in seabed nature.

Keywords : Non-cohesive sand-mud mixtures, Erosion, Suspended sediment transport, Bedload transport, Morphodynamics, Seine Estuary

1. Introduction

Once motion starts, the way particles are transported depends on the size, type, and density of the eroded particles (e.g., [Abbott &](#)

* Corresponding author. IFREMER, DYNECO/DHYSED Laboratory, Centre de Bretagne, CS 10070, 29280, Plouzané, France.

E-mail address: bapt.mengual@hotmail.fr (B. Mengual).

[Francis, 1977](#); [Bagnold, 1966](#); [van Rijn, 1989](#)). In the case of non-cohesive sediment (gravel, sand), sediment particles correspond to individual grains and are likely to experience different transport modes. The larger particles roll on each other causing the so-called bedload process, while the smaller ones undergo saltation, or may even remain in suspension due to the action of upward-moving turbulent eddies. The dynamics of cohesive sediment like mud is more complex due to inter-particle forces, which lead to cohesion

effects (e.g., Winterwerp & van Kesteren, 2004). For cohesive sediment, large lumps of sediment may result from mass erosion and lead to the formation of mud pebbles that roll on the bed, but eroded particles are usually small enough to remain in suspension. The critical particle size between bedload and suspended load regimes increases with external forcing, generally expressed through the bed shear stress.

Computing sediment transport requires the distinction between bedload and suspended load. Bedload is generally tackled through transport capacity, and is usually evaluated empirically as a function of sediment properties and hydrodynamic forcing characteristics (e.g., Meyer-Peter & Müller, 1948; Soulsby & Damgaard, 2005; van Rijn, 2007; Wu & Lin, 2014). Even if several sediment transport models account for bedload and suspended load (e.g. Becherer et al., 2018; Dissanayake et al., 2012), the respective weights of these transport modes on actual bed morphological changes remain poorly documented, in particular in environments where sediment facies consist of non-cohesive/cohesive mixtures. According to the literature, studies on bedload and suspended sediment transport contributions in coastal and estuarine zones mainly concern applications restricted to the surf zone, such as bar morphodynamics or grain-size variability and bed elevation along beach profiles (e.g., Reniers et al., 2013; van der Zanden et al., 2017). Generally, despite lower flux intensities, bedload is considered as a key process likely to induce specific sediment transport pathways that can be essential to represent morphological evolutions of sandbars or sediment sorting in nearshore environments (Reniers et al., 2013; Rivier et al., 2017).

Dealing with the resuspension process, the way the different sediment classes are likely to interact in mixed-sediment beds (i.e., mixtures of cohesive and non-cohesive sediment) is a crucial topic that may have a strong influence on estimates of erosion quantities and subsequent transport patterns. In many studies dedicated to hydro-sediment dynamics modeling, the erosion flux, E , is expressed in a Partheniades form of erosion law (Partheniades, 1965) as shown in Eq. (1). This erosion law involves the bed shear stress, τ , (forcing) and parameters describing erosion characteristics of sediment: the erodibility parameter, E_0 , ($\text{kg}/\text{m}^2/\text{s}$) likely to vary over several orders of magnitude depending on sediment type and granulometry (e.g., Dufois & Le Hir, 2015), the critical shear stress, τ_{ce} , (N/m^2), and the power n representing the potential non-linearity of the erosion flux with the dimensionless excess shear stress.

$$E = E_0 \left(\frac{\tau}{\tau_{ce}} - 1 \right)^n \text{ if } \tau \geq \tau_{ce} \quad (1)$$

$$= 0 \text{ if } \tau < \tau_{ce}$$

Non-cohesive/cohesive sediment interactions can be tackled by discriminating different erosion regimes in which E_0 , τ_{ce} , and n are modulated according to the mud content (mass fraction of mud, f_m). The concept of a critical mud fraction (f_{mcr}) is usually applied to make a distinction between erosion regimes (e.g., Le Hir et al., 2011; Waeles, 2005): when $f_m \geq f_{mcr}$ (i.e. cohesive regime), it is assumed that cohesive effects start to influence the mixture erosion by progressively binding gravel/sand grains, whereas when f_m is lower than f_{mcr} (i.e., non-cohesive regime), it is assumed that the mixtures behave as pure sand and that the mud content does not influence the erosion of non-cohesive particles. However, in the non-cohesive regime, the approach for computing resuspension flux for the different sediment classes within mixtures is not clearly established. Some studies assume a common erosion law for sands and mud (homogeneous erosion of mixtures) and consider average representative E_0 and τ_{ce} values, weighted by the sediment mass fractions within the bed mixture (e.g., Le Hir et al., 2011; Mengual

et al., 2017; Waeles et al., 2007). In this case, strong interactions between sediment classes are assumed. On the other hand, other authors have considered no interactions between sediments, with independent and specific erosion laws for each sediment class, i.e., different erosion parameters E_0 and τ_{ce} (e.g., Franz et al., 2017; Warner et al., 2008). Given the linear dependency of the erosion flux E to E_0 in the erosion law, this choice becomes really important when bed sediment has a multi-modal distribution with the coexistence of non-cohesive and cohesive sediment. In the current study, we focus on the hydro-sediment dynamics and morphological evolutions of the Seine Estuary where gravel, sand and mud coexist within the seabed. Sandy facies are the most abundant over the estuary mouth, which makes the question of erosion modeling in the non-cohesive regime a crucial topic.

The current study presents the set up and application of a three dimensional (3D) process-based numerical morphodynamic model for the Seine Estuary, and aims at assessing:

- (i) how the approach for simulating sediment resuspension in the non-cohesive regime (i.e., homogeneously applied to sediment mixtures through average erosion parameters or independent erosion fluxes considered for each sediment class) can modulate sediment flux and subsequent bed level changes, and
- (ii) the respective contributions of bedload and suspended load in sediment transport and erosion/deposition patterns

The paper is structured as follows. Section 2 presents the Seine Estuary including its main geomorphologic, hydro-sedimentary features, and forcing conditions. Section 3 presents the 3D morphodynamic model used and the numerical modeling experiments. Results are detailed and discussed in Sections 4 and 5, respectively, and main conclusions are summed up in Section 6.

2. The Seine Estuary

The macrotidal Seine Estuary is located in the northwestern part of France and stretches from the Bay of Seine (open to the English Channel) to Poses upstream (P in Fig. 1a). The tide is semidiurnal and the tidal range can be up to 8 m at Le Havre (LH in Fig. 1b). The Seine River flow ranges from 100 to 2300 m^3/s (annual mean: 450 m^3/s) with sediment inputs comprised between 1 and 900 kg/s of sediment, and a mean supply of 23 kg/s corresponding to $725 \times 10^6 \text{ kg}/\text{yr}$ (Schulz et al., 2018). During low river flows, erosion of intertidal flats located in the fluvial part of the Seine Estuary also plays an important role in the downward transfer of fine-grained suspended particulate matter (Deloffre et al., 2005). The main direction of the wind is from the southwest with an average speed of 4 m/s and peaks reaching 15 m/s . At the estuary mouth, dominant waves are from northwest with significant wave heights of 0.5 m on average, reaching up to 3.5 m during energetic conditions.

Using a 3D realistic and validated hydro- and sediment-dynamics model, Grasso et al. (2018) recently assessed the estuarine turbidity maximum (ETM) dynamics in the lower estuary, which has strong effects on sedimentation patterns in subtidal areas and intertidal mudflats. They showed that its location is mainly controlled by the river discharge through the tidal pumping mechanism and salinity gradients, while its mass ($48 \times 10^6 \text{ kg}$ on average, $250 \times 10^6 \text{ kg}$ for spring tide) is linked to the tidal range and can be strongly amplified by wave-induced re-suspension, up to a factor 3 on mean tides. ETM dynamics largely influence sedimentation on mudflats during spring tides (Deloffre et al., 2006).

All these forcings and mechanisms combined with wind-induced circulation drive sediment flux variability and budgets (including sand and mud) of this ETM-dominated estuary (Schulz

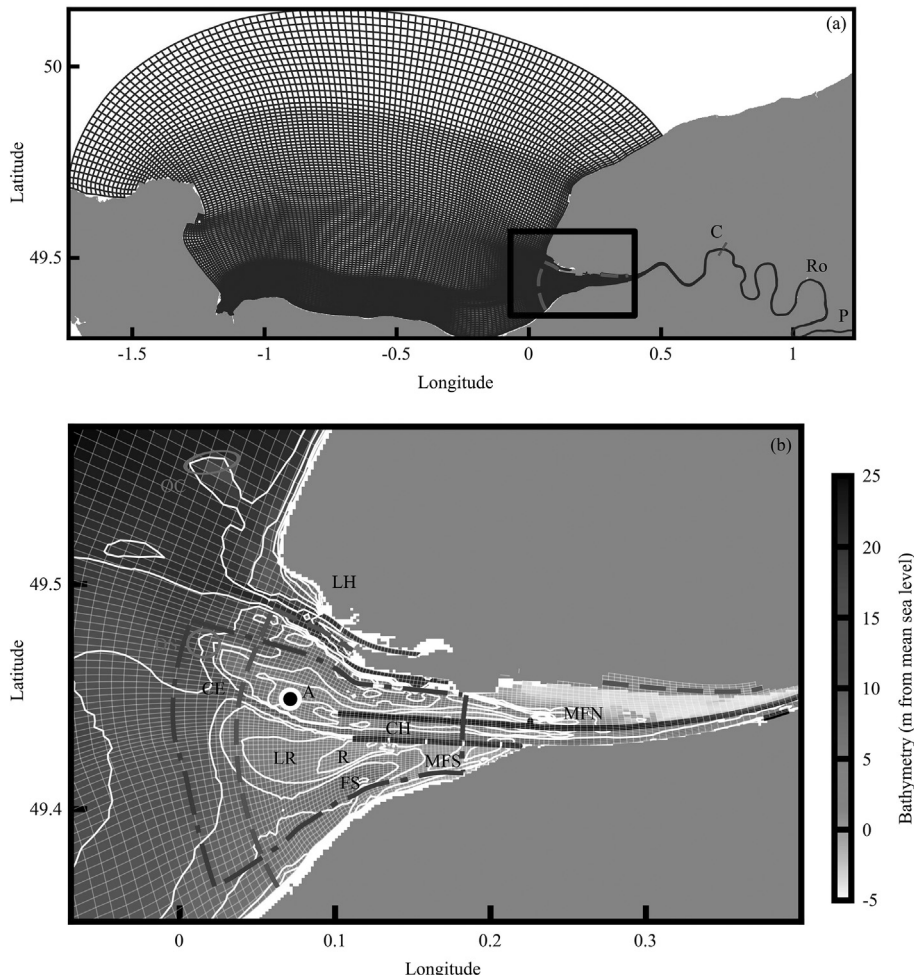


Fig. 1. Geographical extent of the 3D model configuration with its curvilinear non-orthogonal grid in (a), and its bathymetry (in m with respect to mean sea level) over the area of interest in (b). In (b), white contours refer to isobaths (2, 4, 6, 8, 10, 15, and 20 m), dashed line denotes the area (downstream/upstream limits) used to compute the ETM mass (see Section 4). The dash-dotted line refers to a specific area where sediment fluxes are investigated in Section 4. Abbreviations for town and site locations: C, Caudebec, Ro, Rouen; P, Poses; LH, Le Havre; CH, channel; CE, channel entrance; A, Amfard; LR, Les Ratelets; R, Ratier; FS, southern channel; MFN/MFS, northern/southern mudflats; DS, OC dumping sites for dredged sediments (from Rouen navigational channel and from Le Havre harbour and accesses, respectively). The black circle refers to a station of interest mentioned throughout the manuscript.

et al., 2018). Several classes of sediment constitute the bed, including gravel, sand (from coarse to very fine), and mud, given the different sources of sediment coming from the continent and from the sea. Thus, the seabed is characterized by a mosaic of different sediment facies, whose changes are related to forcing variability, resulting in a stratified seabed (e.g., Lesourd et al., 2001).

Since the XIXth century, many engineering works have been undertaken in the Seine Estuary including bank protection by dikes, the associated channelling of the estuary along 120 km, and the expansion of Le Havre (LH) and Rouen (Ro) harbors, respectively, near the mouth and 120 km upstream (see locations in Fig. 1). These works have induced the development of an ebb delta split into two shoals separated by a navigation channel, both prograding seawards (e.g., Waeles et al., 2008). In 2005, a new extension of Le Havre Harbor (“Port 2000”) restricted the total width of the estuary mouth, while the navigation channel along the estuary, up to Rouen, was slightly deepened. The maintenance of navigation channels requires annual dredging up to 6 Mt (Lemoine et al., 2017). In addition, submersible dikes at the mouth, which aimed at enhancing ebb sediment flux, have induced some concentration of the turbidity maximum between these dikes, and some expansion of muddy subtidal areas, while the intertidal mudflats below lateral

wetlands have been considerably reduced (Cuvilliez et al., 2009; Grasso et al., 2018; Grasso & Le Hir, 2019). All these features make the Seine estuary a very dynamic and complex system.

3. Model set up and numerical experiment

3.1. Hydrodynamic models

Current transport patterns and advection of suspended sediment in the Seine Estuary were computed with the 3D MARS model (Lazure & Dumas, 2008). This code solves the primitive equations under classical Boussinesq and hydrostatic pressure assumptions. The model discretization of the Seine Estuary consists of a non-orthogonal curvilinear grid with 10 equidistant sigma-layers (Fig. 1). Its hydrodynamic setting and the realistic forcing used regarding tide constituents (CST France database), meteorological conditions (AROME model; Seity et al., 2011) and river discharge (flow and sediment supply) are the same as those detailed in Grasso et al. (2018) (see Acknowledgments). Regarding turbulence, vertical viscosity and diffusivity for temperature, salinity, and momentum were obtained using the $k - \varepsilon$ turbulence closure of Rodi (1993).

Waves are simulated using the WaveWatchIII model (Roland & Arduin, 2014). Circulation and wave models are run simultaneously and exchange information, every 10 min, thanks to the OASIS-MCT coupler (Craig et al., 2017). The circulation model provides free surface elevation and surface current velocities to the wave model. In return, the wave model provides updated estimates of wave parameters (e.g., bottom orbital velocity and excursion, wave period, wave direction), which enable to compute the wave friction factor, f_w (Soulsby et al., 1993), and the wave-induced skin shear stress on the bed, τ_w , (N/m^2 ; Jonsson, 1966). The total bottom shear stress, τ (N/m^2), was computed according to Soulsby (1997) as a function of τ_w and τ_c , by accounting for the angle between wave and current directions. The latter corresponds to the current-induced shear stress and is provided by the circulation model. Note that τ_w , τ_c , and τ correspond to skin shear stresses, and are computed by accounting for a variable skin roughness length, z_0 . In the current research, it assumed that $z_0 = k_s/30$, where k_s is the so-called Nikuradse roughness parameter taken as $2 \times D_{gs}$, and D_{gs} corresponds to the representative diameter of non-cohesive sediment within the mixture. A minimum z_0 value of 10^{-5} m is defined according to the finest sand class found in the Seine Estuary. Bathymetric changes due to morphodynamics are taken into account in the circulation model and in wave computations.

3.2. Sediment model

The multi-layer/multi-class sediment model coupled with the 3D hydrodynamic model is partly based on the model introduced by Le Hir et al. (2011). Sediment dynamics are computed with an advection-diffusion equation for each sediment class, representing the transport in the water column and sediment exchanges at the water/sediment interface due to erosion/deposition under both wave- and current-induced shear stresses. For more details on the computation of the deposition flux resulting from suspended sediment dynamics, please refer to Grasso et al. (2018).

A multi-layer bed model accounts for corresponding changes within the seabed (e.g., sediment layer composition and thickness). The bed model also accounts for consolidation processes, by solving a Gibson equation for mixed sediment (Grasso et al., 2015). Sediment dredging and dumping operations are explicitly included in the numerical computations, following Lemoine et al. (2017) as follows. When the sediment elevation exceeds the one specified by port authorities, sediment in excess are removed from the seabed and instantaneously released in the bottom layer of the water column at dumping sites (see locations DS and OC in Fig. 1b).

A previous erosion/deposition model for the Seine Estuary had been calibrated by Grasso et al. (2018) to simulate total transport (sand and mud), through the resolution of an advection/diffusion equation. In the current study, this model was upgraded to explicitly simulate bedload, in order to quantify sediment dynamics related to this mode of transport, and to be more realistic for coarse sand and pebble dynamics. In addition, the new model offers different possibilities to model the resuspension of muddy sand mixtures showing a non-cohesive erosion behavior. All these developments are described in the following sections. In the Seine Estuary case, five representative sediment classes were initially distributed according to measured sediment distribution (Lesourd et al., 2016, Fig. 2): gravel (G, 10 mm), coarse sand (CS, 800 μ m), fine sand (FS, 210 μ m), very fine sand (VFS, 100 μ m), and mud (M). The sediment bed is discretized with a maximum of 100 layers of variable thickness ranging from a representative diameter of the local mixture ($dz_{s,min}$) to a maximum value of 10 mm ($dz_{s,max}$). A fusion of deeper layers is operated when the maximum number of layers is reached during deposition. Initially, the bed sediment consists of a 3-m thick compartment homogeneously discretized

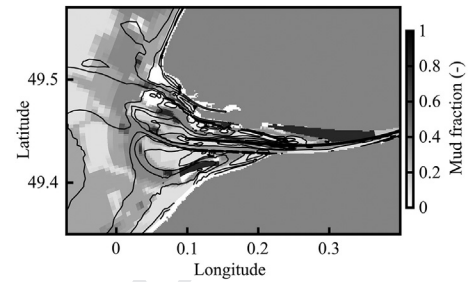


Fig. 2. Sediment initialization, expressed in terms of mud fraction (data from Lesourd et al., 2016). Contours represent the same isobaths as shown in Fig. 1.

along the vertical (50 layers). The bed discretization was chosen as a compromise between the possibility of reproducing thin alternations of sand/mud layers and a reasonable number of layers for computational costs.

3.2.1. Erosion modeling

3.2.1.1. Non-cohesive erosion regime. A non-cohesive erosion regime is assumed when the mud mass fraction, f_m , in the surficial sediment layer is below a critical mud fraction, f_{mcr} , i.e., when there is not enough mud content to trap gravel or sand grains. According to Le Hir et al. (2011), the critical mud fraction value is assumed to increase with the sand diameter as:

$$f_{mcr} = \alpha \cdot D_{gs} \quad (2)$$

where $\alpha = 1000 \text{ m}^{-1}$ and D_{gs} is the average diameter (m) representative of non-cohesive sediment within the mixture. The α value used here corresponds to the lower value proposed by Le Hir et al. (2011), who derived Eq. (2) from experimental tests with $\alpha \in [1000 - 3000 \text{ m}^{-1}]$.

In this non-cohesive regime, it is assumed that gravel can be transported as bedload only, sands as both suspended load and bedload, and mud as suspended load only. The thickness of sediment where grains are likely to be mobilized, the so-called active layer, δ_a , is computed from the formulation of Harris and Wiberg (1997) as a function of the skin bottom shear stress, τ , and D_{gs} . If the thickness of the surficial sediment layer is lower than δ_a , then it is successively merged with underlying sediment layers until the relevant thickness is reached or until a cohesive layer is found (with $f_m > f_{mcr}$).

Resuspension in the non-cohesive regime can be simulated according to two different erosion procedures, hereinafter discussed. In the first option, erosion of the different sediment classes can be considered independently (hereinafter referred to as *eronc_indep* option) for the different sediment classes, k , with specific fluxes E_k (in $\text{kg}/\text{m}^2/\text{s}$) computed following Wu and Lin (2014):

$$E_k = f_k E_{0,k} \left(\frac{\tau}{\tau_{ce,k}} - 1 \right)^{n_k} \quad \text{if } \tau \geq \tau_{ce,k} \\ = 0 \quad \text{if } \tau < \tau_{ce,k} \quad (3)$$

where $E_{0,k}$ is the erodibility parameter of sediment class k (in $\text{kg}/\text{m}^2/\text{s}$), $\tau_{ce,k}$ is the critical shear stress of sediment class k (N/m^2), n_k is a power constant varying with sediment class k ($=1.7$ for sand classes), f_k is the mass fraction of k within the mixture, and τ is the actual bottom skin shear stress (N/m^2). According to Wu and Lin

(2014), the critical shear stress $\tau_{ce,k}$ accounts for hindering/exposure processes and is computed as

$$\tau_{ce,k} = g \cdot \theta_{cri} \cdot (\rho_s - \rho_w) \cdot d_k \cdot \left(\frac{p_{e,k}}{p_{h,k}} \right)^{-m} \quad (4)$$

$$\text{with } p_{h,k} = \sum_{j=1}^N f_j \cdot \frac{d_j}{d_k + d_j} \text{ and } p_{e,k} = \sum_{j=1}^N f_j \cdot \frac{d_k}{d_k + d_j}$$

where g is the gravitational acceleration (m/s^2), ρ_s is the sediment density (2600 kg/m^3), ρ_w is the water density (1025 kg/m^3), θ_{cri} is a critical mobility parameter (0.03), m is an empirical parameter (0.6), d_k ($\text{or } j$) is the diameter of the sediment class k or j (m), f_j is the mass fraction of sediment class j , $p_{h,k}$ and $p_{e,k}$ are the hidden and exposed probabilities for sediment class k , respectively, and N is the total number of gravel/sand classes.

The erodibility parameter for sand classes is expressed as

$$E_{0,k} = C_{E0} \rho_s \frac{W_{s,k} \cdot d_k}{\delta} \quad (5)$$

where $W_{s,k}$ is the settling velocity of the sediment class k (m/s ; Eq. 102 in Soulsby, 1997) and δ is the reference level, which is the elevation above the bed where both erosion and deposition fluxes are expressed, arbitrarily chosen as 0.02 m. In Eq. (5), C_{E0} refers to a constant value set at 0.0024, which is slightly lower than the one prescribed by Wu and Lin (2014). This choice was made in order to minimize differences with previous work and to achieve validation from Grasso et al. (2018) regarding sand erosion rates, in particular for fine sand (FS), which is dominant at the estuary mouth.

For mud, the erosion rate is computed from Eq. (3) with $E_{0,k} = E_{0,mud} = 3 \times 10^{-4} \text{ kg/m}^2/\text{s}$ and $n_k = n_{mud} = 1$, which correspond to calibration parameters used by Grasso et al. (2018). $\tau_{ce,mud}$ is defined as the average critical shear stress representative of sand classes in the mixture.

In the second option, the erosion law in the non-cohesive regime is applied homogeneously to the mixture (hereinafter referred to as *eronc_mix* option), by considering representative average values, weighted by sediment mass fractions, of E_0 ($= \sum f_k \cdot E_{0,k}$), τ_{ce} ($= \sum f_k \cdot \tau_{ce,k}$) and n in Eq. (1). This option implies that sand and mud are eroded at the same rate according to their respective fractions in the mixture. For the *eronc_mix* option, n is equal to 1.7 for all sediment classes.

3.2.1.2. Transitional to cohesive erosion regime. When $f_m \geq f_{mcr}$, it is assumed that mud starts to influence non-cohesive sediment erosion due to cohesive effects, which become more important when f_m increases. In this transitional regime, sediment transport occurs in suspension only and erosion is applied homogeneously to sediment mixtures (as in the *eronc_mix* option) for successive sediment layers without the preliminary step of active layer mixing. The erosion flux is computed using Eq. (1) by considering average erosion parameters, E_0 , τ_{ce} , and n , representative of bed mixtures (weighted by the sediment mass fractions). According to Mengual et al. (2017), an exponential transition of erosion parameters is prescribed between non-cohesive and cohesive regimes. First, average erosion parameters representative of the gravel/sand matrix ($E_{0,gs}$, $\tau_{ce,gs}$, n_{gs}) are computed independently of muddy sediment. Then, erosion parameters related to any gravel-sand-mud mixture showing a mud fraction $f_m \geq f_{mcr}$ is computed as

$$X_{tr} = (X_{gs} - X_{mud}) \cdot e^{C_e \cdot (f_{mcr} - f_m)} + X_{mud} \quad (6)$$

where X_{tr} refers to erosion parameters representative of the whole mixture in the transitional regime ($E_{0,tr}$, $\tau_{ce,tr}$, n_{tr}), $X_{gs} = (E_{0,gs}$, $\tau_{ce,gs}$, $n_{gs})$, $X_{mud} = (E_{0,mud}$, $\tau_{ce,mud}$, $n_{mud})$, and C_e is a coefficient function of f_{mcr} controlling the rapidity of the transition. Based on experimental results of Le Hir et al. (2011), the C_e coefficient is defined as $C_e = 78.5 f_{mcr} - 2$ ($= 78.5 \times 10^3 D_{gs} - 2$). This relation implies that if the non-cohesive matrix becomes coarser, mud will start to influence the entire mixture erosion for a higher mass fraction, f_m , and the transition towards a pure mud erosion behavior will be faster. In this transitional regime, $\tau_{ce,mud}$ is computed as a function of the relative mud concentration (mud concentration in the space between non-cohesive grains) according to Grasso et al. (2018). It should be noted that when f_m substantially exceeds f_{mcr} , the first term in Eq. (6) becomes negligible, and a fully cohesive regime is reached.

3.2.2. Modeling of bedload transport

For gravel and sand classes, bedload flux ($q_{b,k}$ in kg/m/s) is computed using the formulation of Wu and Lin (2014):

$$q_{b,k} = 0.0053 \rho_s f_k \sqrt{\left(\frac{\rho_s}{\rho_w} - 1 \right)} \cdot g \cdot d_k^3 \left(\frac{\tau}{\tau_{ce,k}} - 1 \right)^{2.2} \quad (7)$$

Note that in Eq. (7), $\tau_{ce,k}$ is computed using Eq. (4) by accounting for hindering/exposure processes over all gravel/sand classes, as for resuspension. Following the procedure described by Rivier et al. (2017), bedload flux has the same direction as the bed shear stress, τ , and thus, is projected along the x and y directions of the grid ($q_{bx,k}$ and $q_{by,k}$). $\Delta_{b,k,out}^{ij}$, the mass of sediment class k leaving a cell (i, j) during a time step, dt , for bedload is expressed as

$$\Delta_{b,k,out}^{ij} = \left| q_{bx,k}^{ij} \cdot dy^{ij} \cdot dt \right| + \left| q_{by,k}^{ij} \cdot dx^{ij} \cdot dt \right| \quad (8)$$

where the $||$ operator refers to absolute value, and dx^{ij}/dy^{ij} to the cell sizes along x/y directions. Bed slope effects are prescribed through the approach described by Lesser et al. (2004).

According to the procedure of Rivier et al. (2017), the bedload mass of sediment class k , $\Delta_{b,k,in}^{ij}$, getting into the cell (i, j) during dt is

$$\Delta_{b,k,in}^{ij} = \left(\max \left\{ q_{bx,k}^{i-1,j}; 0 \right\} - \min \left\{ q_{bx,k}^{i+1,j}; 0 \right\} \right) \cdot dy^{ij} \cdot dt + \left(\max \left\{ q_{by,k}^{i,j-1}; 0 \right\} - \min \left\{ q_{by,k}^{i,j+1}; 0 \right\} \right) \cdot dx^{ij} \cdot dt \quad (9)$$

Such a treatment of bedload by considering first an extraction of sediment from the cell equal to the bedload rate multiplied by the time step and then an input of sediment from adjacent cells corresponds to an explicit upwind scheme of bedload transport.

3.3. Model validation

A validation work was done by Grasso et al. (2018) for a previous version of the model (applied on a similar configuration) in terms of water levels, waves, salinity, currents, and suspended particulate matter dynamics over the zone of interest (from the estuary mouth to upstream locations). New developments specific to this work and, in particular, the approach for computing re-suspension and bedload flux according to the formulations of Wu and Lin (2014) are likely to modulate the sediment dynamics previously validated by Grasso et al. (2018). The relevance of the current model results will be assessed through comparisons in terms of morphological changes and ETM dynamics.

3.4. Numerical experiments

Three simulations have been done over a 2-year period (2011–2012). The first year, excluded from all analyses, can be considered as a spin-up period needed to adjust the seabed nature and morphology with actual currents and waves on one hand, and to develop and stabilize hydrological structures (e.g., salinity patterns) on the other hand. All simulations have been analysed over the second year simulated which was selected based on the representativeness of its temporal distributions of significant wave height, wind speed, and river discharge, compared to those obtained over the 2009–2016 period.

The first simulation (hereinafter referred to as Run 1) does not account for bedload transport and considers that re-suspension flux in the non-cohesive regime (when $f_m < f_{mcr}$) is applied homogeneously to the mixture (*eronc_mix* option; see Section 3.2.1.1). The second simulation (Run 2) again does not include bedload transport but considers independent erosion of the different sediment classes in the non-cohesive regime (*eronc_indep* option). Lastly, the third simulation (Run 3) accounts for bedload transport and the *eronc_indep* option in the non-cohesive erosion regime.

4. Results

The three simulations described in Section 3.4 are compared in terms of suspended sediment dynamics and morphologic evolution in order to assess the sensitivity of model results to the approach for simulating sediment resuspension in the non-cohesive regime on one hand, and the contribution of bedload to morphodynamics on the other hand.

4.1. Suspended sediment dynamics: sensitivity to erosion in the non-cohesive regime

4.1.1. Sediment fluxes

Model results (hourly outputs) from Runs 1 and 2 are first compared in terms of depth-averaged suspended sediment flux, by focusing on the residual dynamics through the application of a numerical filter (Demerliac, 1974) extending over ± 36 h that

enables tidal oscillations to be removed. Run 1 corresponds to homogeneous erosion (*eronc_mix* option) while Run 2 considers independent (*eronc_indep* option) erosion fluxes of sediment classes in the non-cohesive regime. Fig. 3 illustrates a comparison of the 50th-percentile of residual sediment fluxes derived from these two runs over the year 2012, hereinafter referred to as “average” fluxes. Substantial increases in sand and mud fluxes are derived when erosion is applied homogeneously to the mixture, in comparison to fluxes obtained by considering independent erosion of the different classes (Fig. 3). These differences are especially noticeable over Shoals LR, R, and A. Over the area including shoals and most of the estuary mouth, correlation diagrams of sediment flux magnitudes show that average sand and mud fluxes derived from the run considering homogeneous erosion are 2 times and 30% larger, respectively (Fig. 4). These contrasts can be related to the sensitivity of erosion flux in the non-cohesive regime to erosion parameters prescribed in the erosion law, especially the erosion parameter E_0 (Eq. (5)) which varies by several orders of magnitude as a function of sediment granulometry or type. Thus, considering a representative average E_0 value in the *eronc_mix* case can result in more erosion of fine sediment classes, especially VFS and M, due to the presence of coarser sediment within the mixture likely to increase erosion rates, and thus, sediment fluxes. For instance, Fig. 4d highlights that the increase of mud flux due to homogeneous erosion is more pronounced when the bed median diameter becomes larger. Note that d_{50} refers to the 50th-percentile (i.e., the median) diameter of the surficial sediment computed over the 2012 year, and extracted over the same zone as for the average sediment flux (i.e., dash-dotted line on Fig. 1b). This result also is clearly visible in Fig. 5 which illustrates temporal changes of resuspension flux for all sand classes and mud in Runs 1 and 2 at a station located over Shoal A (black dot on Fig. 1b) during a 4-month period. When the fraction of CS increases in the surficial sediment, resuspension fluxes of FS, VFS, and M are substantially higher in Run 1 that considers homogeneous erosion. Note that these larger resuspension fluxes result in more pronounced erosion of the sediment bed, increased by 10 cm during the 4-month period and by 20 cm over the whole year, which represents a two-fold increase (Fig. 5g). Since erosion occurs in the non-cohesive regime most of the time in all simulations, such increases of re-suspended dynamics of fine

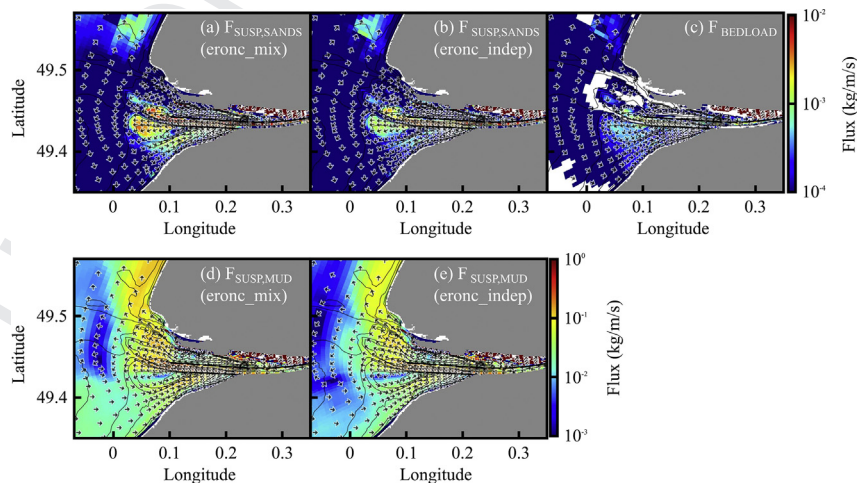


Fig. 3. Maps of the 50th-percentile of residual sediment flux (kg/m/s) over the whole simulated year (2012): depth-averaged sediment flux in suspension for all sand classes ($F_{susp,sands}$) and mud ($F_{susp,mud}$) for the *eronc_mix* option in (a, d, respectively) and the *eronc_indep* option in (b, e, respectively) in the non-cohesive regime; bedload flux (Run 3) in (c). Contours represent the same isobaths as in Fig. 1.

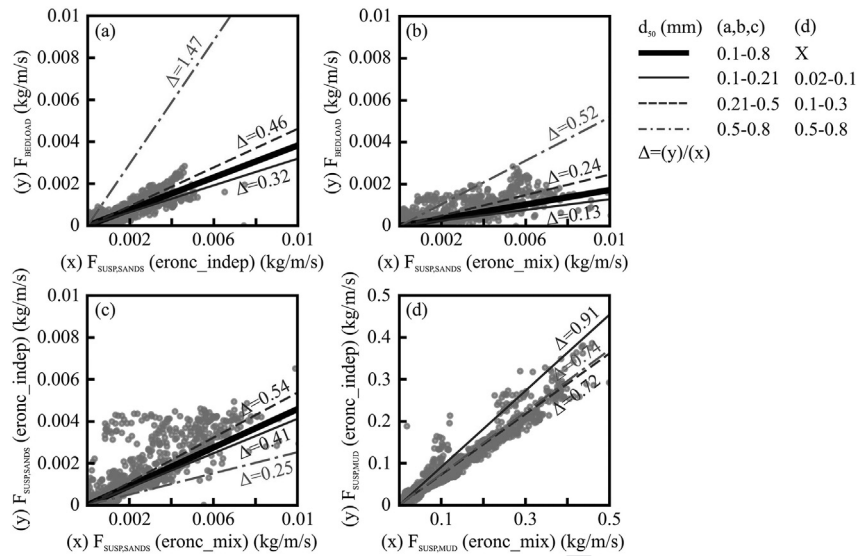


Fig. 4. Correlation diagrams between: bedload flux ($F_{bedload}$) and depth-averaged suspended sand flux ($F_{susp, sands}$) derived from Run 2 (*eronc_indep*) and Run 1 (*eronc_mix*) in (a) and (b), respectively; (c) suspended sand flux from Runs 1 and 2; (d) suspended mud flux ($F_{susp, mud}$) from Runs 1 and 2. Correlations are done on the magnitude of the 50th percentile of residual sediment flux over the year 2012. On each subplot, grey dots are the flux value associated with each model cell contained in the area delimited by the dash-dotted line in Fig. 1b. The different regression lines are computed for different ranges of d_{50} , which corresponds to the 50th-percentile of the surficial sediment diameter (1 mm integration) computed over the same year and extracted over the same zone as the sediment flux.

sediment due to the presence of coarser sediment within bed mixtures may have important implications in the resulting seabed nature changes and morphological evolution (Section 4.2).

Fig. 3 also provides a comparison between residual average suspended sand flux ($F_{susp, sands}$) and the residual average bedload flux ($F_{bedload}$). Gradients in sediment flux are consistent between suspended load and bedload dynamics, with larger fluxes occurring over ebb delta shoals (*LR* and *A*) and in the main channel, i.e., in areas influenced by waves and tidal currents. However, suspended sand fluxes (Fig. 3a and b) dominate those caused by bedload (Fig. 3c), whatever the way of modeling resuspension in the non-cohesive regime. The relative contribution of bedload, $F_{bedload}/F_{susp, sands}$, is weaker when suspended sediment flux results from homogeneous erosion in the non-cohesive regime, $F_{susp, sands}$ associated with the *eronc_mix* option being higher than in case of the *eronc_indep* option. This is consistent with the more pronounced erosion dynamics highlighted with the *eronc_mix* option. From the correlation diagrams, it appears that $F_{bedload}$ represents 17% of $F_{susp, sands}$ in the case of the *eronc_mix* option (Fig. 4b), while it represents 38% in the *eronc_indep* case (Fig. 4a). It can be noticed that the bedload contribution increases when bed sediment becomes coarser, as expected. For instance, over areas characterized by a d_{50} ranging from 0.5 to 0.8 mm, $F_{bedload}$ increases and becomes 1.5 times larger than the $F_{susp, sands}$ derived with the *eronc_indep* option.

Interestingly, the average orientation of residual bedload flux differs from the orientation related to suspended sediment flux over some areas. For instance, $F_{bedload}$ exhibits a more pronounced southward component over the Shoal *LR*. At the western boundary of Shoal *LR*, a convergent sediment transport due to bedload can be noticed (eastward offshore fluxes, southwestward fluxes on the shoal), not visible in suspended sediment flux patterns.

4.1.2. Estuarine turbidity maximum (ETM)

The total ETM mass is compared between Runs 1 and 2 and the mean value computed by Grasso and Le Hir (2019), see Fig. 6. This integrated parameter is a good proxy to investigate mud dynamics

at the estuary scale. In the current case, it corresponds to the integration of suspended sediment mass of mud over a zone that includes most of the estuary mouth (downstream/upstream limits corresponding to the dashed line on Fig. 1), where the ETM is known to be present. Within the same limits, Grasso and Le Hir (2019) computed (over a 1-year period) a mean ETM mass of 75×10^6 kg with peaks of $300 (\pm 50) \times 10^6$ kg occurring during spring tides or stormy conditions. The ETM mass over the simulated year is shown in Fig. 6 for Runs 1 and 2. Both simulations highlight ETM dynamics influenced by neap/spring tide alternations and subject to storm-induced peaks, and an average ETM mass consistent with the one described by Grasso and Le Hir (2019). However, the average ETM mass value obtained from Run 2 (independent erosion in the non-cohesive regime), 72×10^6 kg, appears closer to the “reference value” from Grasso and Le Hir (2019) than the mean ETM mass derived from Run 1 (homogeneous erosion), 90×10^6 kg. Note that the higher ETM mass in Run 1 appears to be consistent with more pronounced sediment fluxes highlighted in Section 4.1.1.

4.2. Erosion/deposition patterns

Bed level changes (i.e., erosion/sedimentation patterns) derived from the different runs over the simulated year are shown in Fig. 7. Bathymetric changes measured between late 2010 and late 2012 are included in Fig. 7d to provide an idea of actual average morphological trends at the estuary mouth. The observed morphological changes are expressed in m/y to make the comparison with simulated trends easier.

4.2.1. Effect of the erosion mode for non-cohesive sediment

Significant differences in erosion/deposition patterns (Fig. 7) can be underlined between Run 1 (*eronc_mix*) and Run 2 (*eronc_indep*). Run 1 exhibits more pronounced erosion on shoals located on both sides of the channel, especially over the southern part of Shoal *A* and the external contour of Shoal *LR*. In addition, more sedimentation occurs over all accretion areas in Run 1, for

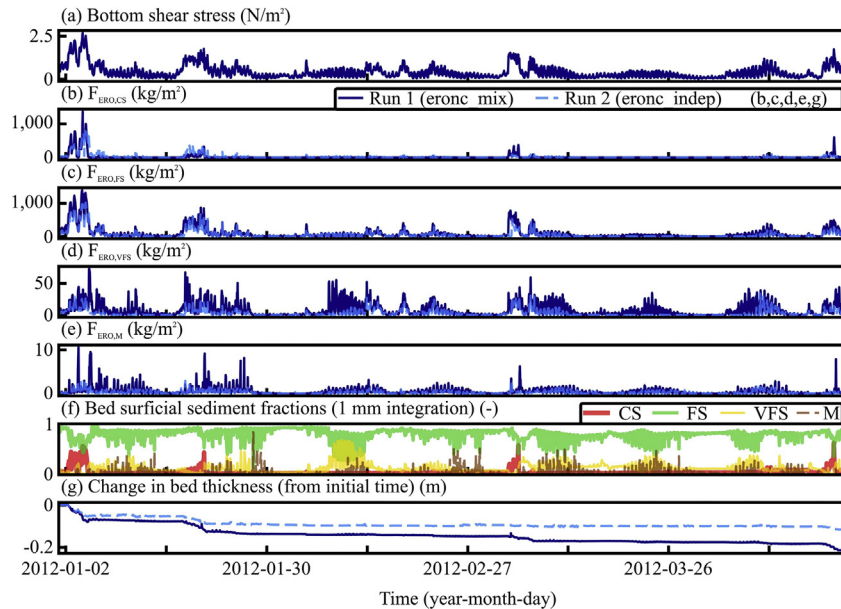


Fig. 5. Temporal series of bottom shear stress (a), erosion flux (in kg/m²) for coarse sand (CS) (b), fine sand (FS) (c), very fine sand (VFS) (d), mud (M) (e), and changes in bed thickness (in m) (g) for Run 1 (*eronc_mix* option, solid line) and Run 2 (*eronc_indep* option, dashed line). Surficial sediment fractions (1 mm integration) shown in (f) refer to Run 1. The station is located over the Shoal A (latitude = 49.449 N; longitude = 0.071 W; see black dot in Fig. 1b).

instance over the northern part of Shoal A, over Shoal R, or in the northern channel (to the north of dikes delimiting the main navigational channel). More pronounced bed level changes highlighted in Run 1 (homogeneous treatment of resuspension in the non-cohesive regime) are consistent with higher sediment flux and ETM mass described in Section 4.1. In addition, simulated erosion occurs in the non-cohesive regime most of the time over the estuary mouth, which amplifies differences between morphological evolutions of Runs 1 and 2. These differences of erosion/deposition patterns lead to differences in average surficial seabed nature (not illustrated here): when the erosion of non-

cohesive sediment mixtures is homogeneous (Run 1), bed sediment over areas subject to erosion is generally coarser whereas it tends to be finer over deposition zones.

4.2.2. Bedload contribution

The influence of bedload processes for non-cohesive sediment (G, CS, FS, and VFS) does not substantially change the erosion/deposition patterns (difference between Run 2 [without bedload] and Run 3 [with bedload] in Fig. 7): erosion is slightly enhanced on Shoals LR/A, and more deposition occurs in some locations, for instance to the north of Shoal A.

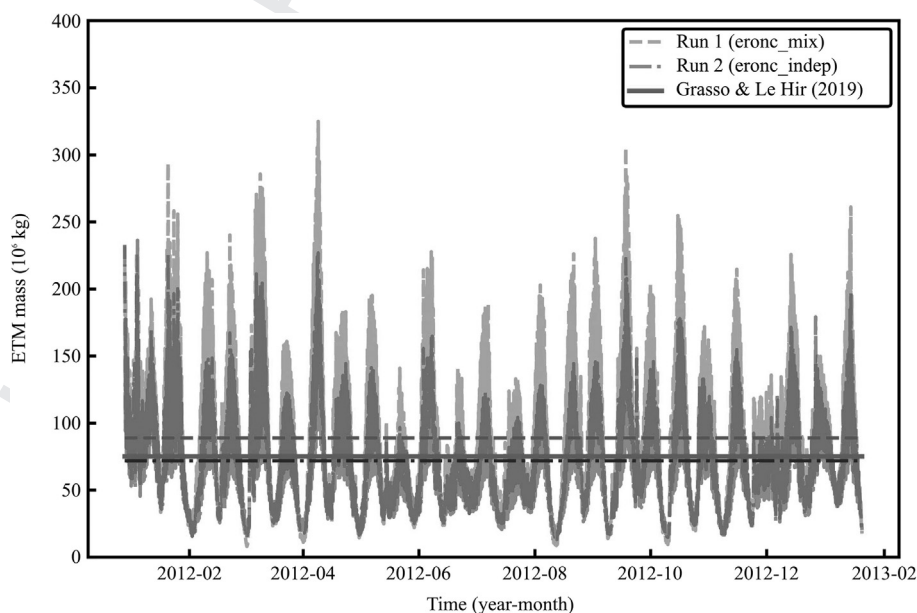


Fig. 6. ETM mass (zone considered for integration: dashed line on Fig. 1) derived from Run 1 (*eronc_mix* option) and Run 2 (*eronc_indep* option) over the simulated year. The dashed, dash-dotted, and solid horizontal bars refer to average ETM masses derived from Runs 1 and 2 over the year 2012, and obtained by Grasso and Le Hir (2019) over the same zone from a 1-year simulation, respectively.

In addition to bed level changes, the bedload contribution can be quantified on sediment mass exchanges. Mass budgets (in kg/m²) relative to sand erosion/deposition, mud erosion/deposition, and divergences resulting from bedload ($Bud_{susp, sands}$, $Bud_{susp, mud}$, $Bud_{bedload}$, respectively) have been computed in each (i, j) cell (with area $S^{i,j}$) as follows:

$$Bud_{bedload} = \int_t \left(\sum_k \left[\Delta_{b,k,in}^{i,j} - \Delta_{b,k,out}^{i,j} \right] / S^{i,j} \right) \quad (10)$$

= G, CS,
FS, VFS

and

$$Bud_{susp,k} = \int_t (D_k^{i,j} - E_k^{i,j}) \cdot dt \quad (11)$$

$$Bud_{susp,sands} = \sum_{(k=CS,FS,VFS)} Bud_{susp,k} \quad (12)$$

$$Bud_{susp,mud} = \sum_{(k=M)} Bud_{susp,k} \quad (13)$$

where D_k is the deposition flux (Krone, 1962) and E_k is the erosion flux of the sediment class k . These mass budgets represent either vertical fluxes or divergences of bedload-induced fluxes, all of them cumulated over the yearly period (Fig. 8). Suspended transport of sand (especially FS and VFS) is responsible for most of sediment mass variations over the 1-year period ($Bud_{susp, sands}$ in Fig. 8a), especially in comparison with budgets related to muddy sediment ($Bud_{susp, mud}$ in Fig. 8b). This feature can be explained by the abundance of sand classes in sediment facies at the estuary mouth. Although not being dominant, the mass budget due to bedload

appears to be significant (Fig. 8c). Remarkably, bedload-induced mass variations follow those due to suspended sediment transport over most of the estuary mouth (red areas in Fig. 8d). Relative contributions of bedload to total mass budgets are around 25% over large erosion areas such as Shoals LR and A, and can even become higher in sedimentation zones like between R and FS, or at the north of A. However, mass variation trends caused by bedload can locally differ from those linked to suspended sediment dynamics (blue areas in Fig. 8d). For instance, mass budgets reveal that bedload promotes sediment accretion on the south-southwest part of Shoal LR, whereas suspended sediment dynamics lead to residual erosion. A slight change in the average bed granulometry due to bedload (50th percentile of d_{50}) also can be noticed: areas where bedload promotes accretion (e.g., positive mass budget area appearing in yellow in Fig. 8c, like Shoal LR) are associated to a noticeable coarsening of surficial sediment, which results from the residual transport of medium to coarse sand towards the south-southwest occurring on the northern/mid parts of Shoal LR (Fig. 3c).

5. Discussion

5.1. Erosion mode in the non-cohesive regime

Many coastal environments, like the Seine Estuary, are characterized by seabeds containing different sediment types and classes that are likely to interact and influence erosion processes and subsequent transport patterns. These interactions can occur in different manners like hindering/exposure or bed armoring processes, and become complex between non-cohesive (gravel, sand) and cohesive (mud) sediments through the development of cohesive effects. The current study assessed the influence of sediment interactions on the resuspension process when the seabed mud content f_m is not enough to influence the erosion of non-cohesive particles (non-cohesive regime).

Despite that it is generally admitted that in the non-cohesive regime sediment particles behave like sand (e.g., Waeles, 2005), the approach for computing resuspension flux for the different

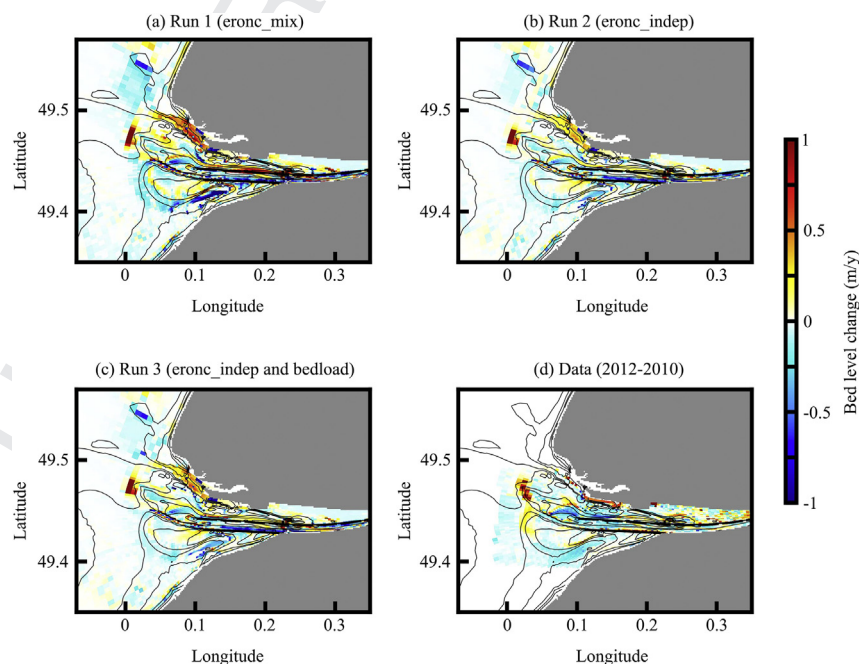


Fig. 7. Bed level changes (in m/y; erosion if < 0, sedimentation if > 0) over the 2012 year for (a) Run 1 (*eronc_mix* option without bedload), (b) Run 2 (*eronc_indep* option without bedload), (c) Run 3 (*eronc_indep* option with bedload), and over the 2010–2012 period for measurements in (d). Contours represent the same isobaths as in Fig. 1.

sediment classes within mixtures is not clearly established. This is a crucial topic and the question remains open. Some studies have assumed a common erosion law for sand and mud (homogeneous erosion of mixtures) in the non-cohesive regime (e.g., Le Hir et al., 2011; Mengual et al., 2017; Waeles et al., 2007). In this case, the erosion parameters involved in resuspension flux computations are likely to depend on the sand distribution and on the mud content. Based on observations from Mitchener and Torfs (1996), Waeles (2005) proposed a linear increase of τ_{ce} with the increasing mud content in the non-cohesive regime (relation used in other studies, e.g., Bi & Toorman, 2015; Carniello et al., 2012). Other studies differentiate sand and mud resuspension fluxes with specific laws (Carniello et al., 2012; Dufois et al., 2014; van Ledden, 2003; van Ledden et al., 2004), often by considering interactions between sediment classes. For instance, van Ledden (2003) computes mud erosion flux as a function of bedload transport rate and the saltation length of sand particles. Lastly, some studies have considered independent and specific erosion laws (different erosion parameters) for each sediment class (e.g., Franz et al., 2017; Warner et al., 2008).

The current study focused on the sediment dynamics of the Seine Estuary and revealed erosion/deposition patterns closer to observed ones when independent resuspension fluxes are considered in the non-cohesive regime. Considering a unique erosion law for all sediment classes in the non-cohesive regime (pure sand erosion behavior) requires a rule for formulating erosion parameters. When the mixture erosion parameters are deduced from the individual erosion parameters of each class, averaged by considering their sum weighted by the respective mass fractions, model results exhibit higher sediment fluxes and morphological changes, which generally are overestimated compared to observations. This overestimation is directly related to the high variability (several orders of magnitude) of E_0 values depending on sediment types and diameters, which vary from for $O(10^{-2})$ $\text{kg/m}^2/\text{s}^1$ (coarse sand) to $O(10^{-4})$ $\text{kg/m}^2/\text{s}^1$ (very fine sand and mud). Therefore, the use of an average E_0 in the erosion law leads to higher resuspension fluxes for

the finest sediment due to the presence of coarser sediment particles in the mixture. Our results suggest that when sediment grain-size distributions become heterogeneous and multimodal regarding non-cohesive particles, an independent treatment of resuspension fluxes for each sediment class is more appropriate.

In the current study, sediment interactions in the non-cohesive erosion regime occur through the critical shear stress. For sand, hindering/exposure processes due to grain size heterogeneity are taken into account in τ_{ce} estimates (Eq. (4)). In agreement with Rivier et al. (2017), hindering/exposure processes have significant effects on the vertical and horizontal sorting of bed sediment. In the current case, hindering/exposure processes limit and smooth spatial gradients in bed granulometry. For mud, it is assumed that its consolidation state does not control the initiation of motion if sand classes are dominant in the mixture. Fine muddy particles are assumed to be mobilized as soon as sandy or gravel particles begin to move: then τ_{ce} for mud corresponds to a weighted average of sand critical shear stresses. Interestingly, Franz et al. (2017) considered that the critical shear stress of mud in the non-cohesive regime is equal to the minimum critical shear stress of sand particles. The underlying concept is the same: when sandy particles start to move, mud trapped in the non-cohesive matrix is resuspended. However, when the fraction of the finest sand in bed material is low with most of muddy particles trapped between coarser sands, applying the critical shear stress of this finest sand to muddy particles is likely to enhance the mud resuspension. For instance, in the current case, this hypothesis amplifies erosion trends over key regions, such as shoals, which result in over-estimated bathymetric changes compared to observations. Dealing with mud dynamics, another interesting alternative would be to assume a variation of the mud erodibility parameter (E_0) as a function of the characteristics of sand classes in the mixture, as proposed by van Ledden (2003). More generally, the erosion behavior of muddy particles in the non-cohesive regime is a key point that deserves further research.

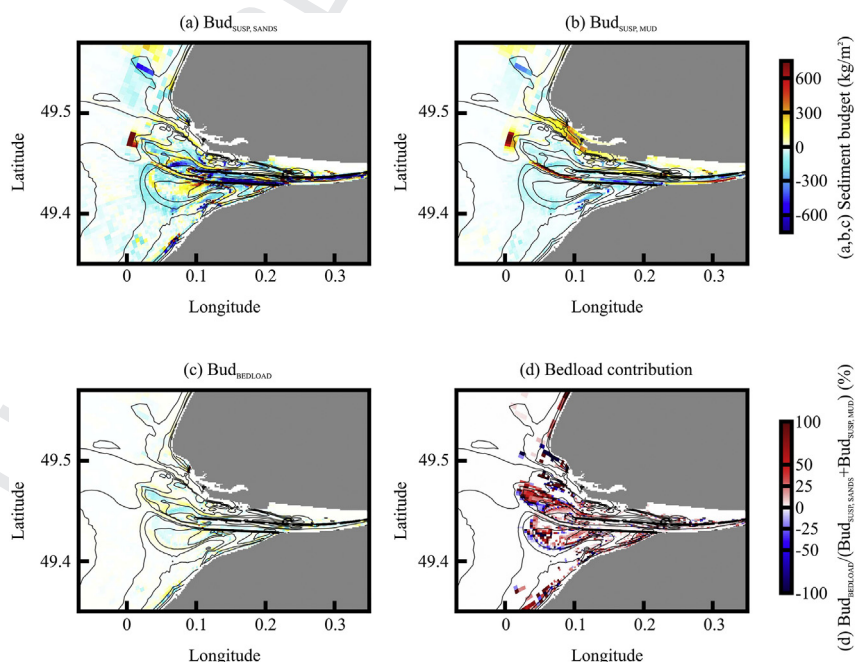


Fig. 8. Annual mass budgets (Run 3; in kg/m^2) due to residual suspended sediment transport ($Bud_{susp, sands}$ (a) and $Bud_{susp, mud}$ (b) for all sands and mud, respectively) and bedload, $Bud_{bedload}$ (c). The bedload contribution in (d) corresponds to ratio (c)/(a+b) expressed in percent. Contours represent the same isobaths as in Fig. 1.

5.2. Bedload contribution to sediment dynamics

In the current application, bedload transport appears as a non-dominant, but significant contributor to the sediment dynamics of the Seine Estuary, as it influences horizontal fluxes, erosion/deposition patterns, and seabed nature changes. Furthermore, increases in the sediment mass budgets of 25–30% over shoals suggest that bedload may have more important implications on bed morphology over longer periods. For instance, bedload contributions are likely to increase at locations where sediment granulometry exhibits coarsening trends over time. Indeed, accounting for bedload becomes more important when the proportion of coarse particles in the seabed increases. Jacobsen and Fredsoe (2014) highlighted that the ratio between maximum suspended load and bedload transport decreases by one order of magnitude with an increase in the grain diameter by a factor 2 (from 0.2 to 0.4 mm).

In the current case, bedload contributions to sediment dynamics is dependent on the approach for modeling resuspension in the non-cohesive regime (sediment classes eroded homogeneously or independently). A substantial decrease of the bedload contribution is noted when erosion is applied homogeneously to the mixture. Changes in bed morphology caused by bedload (erosion/deposition trends) are generally consistent with those resulting from suspended sediment transport over the estuary mouth. However, some specific patterns resulting from bedload appear in the current simulations regarding erosion/deposition patterns and changes in bed composition. For instance, bedload induces a slight increase of the average bed granulometry along the southern border of the Shoal LR, associated with a positive sand mass budget (i.e., residual deposition) which almost counterbalances the residual erosion caused by resuspension. This result is consistent with several studies dedicated to nearshore sandbar morphodynamics (Franz et al., 2017; Reniers et al., 2013; Rivier et al., 2017; van der Zanden et al., 2017), which highlighted that bedload and suspended load can be responsible for contrasted preferential sediment transport pathways leading to different but complementary changes in morphology (e.g., bedload-induced onshore bar migration) and seabed nature (e.g., cross-shore sediment sorting over surf zones).

In the current study, bedload has been prescribed according to Wu and Lin (2014), based on the previous relation proposed by Wu et al. (2000) under a current forcing only. This formulation has demonstrated its relevance through an extensive validation efforts done over a large number of experimental datasets from the literature. Blanpain (2009) showed that the formulation of Wu et al. (2000) was the best to reproduce observed motion of different sediment classes at the seabed interface in the Normand-Breton Gulf. Durafour et al. (2015) compared several formulations of bedload transport to flux observations over heterogeneous gravel/sand beds, and found that the one from Wu et al. (2000) was the most accurate. In addition, Guérin et al. (2016) demonstrated the ability of the formulation of Wu and Lin (2014) to capture complex morphological changes of sandbanks in variable nearshore environments (tide or wave dominated). However, many other popular formulations exist and could be compared in future research (e.g., Meyer-Peter & Müller, 1948; Soulsby & Damgaard, 2005; van Rijn, 2007). Bedload transport occurring at the water/sediment interface may be substantially modified by bed slope, both in terms of magnitude and direction (Bagnold, 1966). In the current application, based on the formulation from Lesser et al. (2004), it appears that bed slope has small effects on

bedload flux and resulting erosion/deposition patterns, at least at the time scale investigated.

5.3. Relevance of simulated morphological evolutions

Even though measured bed level changes shown in Fig. 7d do not cover the same period as the simulations, they provide insight on average morphological changes during two years (including the simulated year). In addition, other observed bathymetric changes obtained throughout different and larger periods (2008–2012, 2008–2018) have shown that morphodynamic trends highlighted between 2010 and 2012 are very representative of general conditions in the Seine Estuary.

Considering homogeneous resuspension in the non-cohesive regime (Run 1; *eronc_mix* option; Fig. 7a) leads to overestimated morphological evolutions compared to observations, both in terms of erosion and deposition patterns. Remarkably, simulated morphodynamic trends derived from Run 3 considering the *eronc_indep* option (independent erosion of sediment classes; Fig. 7c) are, on average, in fair agreement with observations in terms of magnitude and spatial distribution, in particular over shoals (e.g., A and R), mud flats and channels (main and FS channels).

The dumping site DS, where dredged sediment from the Rouen Navigation Channel are dumped, appears very distinctly on both simulated and observed maps of bed level changes (area of high sedimentation). Based on the procedure from Lemoine et al. (2017) and Grasso et al. (2018), the current model reproduces well the amounts of sediment dredged by Ro/LH (see Fig. 1) harbor authorities, i.e., ~6 Mt/y according to Lemoine et al. (2017).

5.4. Model limitations

The coupling between hydrodynamic and wave models from the OASIS-MCT coupler enables to account for the changes of water depth and currents in the wave computations. This appears to be very important to accurately compute the bottom shear stress, that controls the sediment erosion. However, waves also induce specific 3D circulations over near-shore shallow areas (e.g., Guérin et al., 2018; Zheng et al., 2017). Waves are likely to substantially influence the orientation and shear linked to currents, the resulting sediment transport, and consequently, morphological evolutions (van Rijn et al., 2013). This should require further investigations in future research.

6. Conclusions

The aim of the current study was twofold:

- to evaluate the respective contributions of bedload and suspended load in sediment dynamics and subsequent morphological changes in a mixed-sediment environment (the Seine Estuary),
- to assess how these dynamics are influenced by the approach for simulating sediment resuspension when non-cohesive particles are dominant within mixtures (non-cohesive regime).

A 3D process-based morphodynamic model was implemented and numerical simulations were done under realistic forcing (including tide, waves, wind, and river discharge) and different scenarios for a time period of one year.

At the estuary mouth, the overall sediment dynamics are substantially modified and generally enhanced (especially over shoals)

when resuspension in the non-cohesive regime is applied homogeneously to bed mixtures by averaging erosion parameters of the different particle classes, in comparison with the case considering independent erosion of these different classes. Considering a representative average erodibility parameter in the erosion law (weighted by mass fractions) in the homogeneous erosion case results in more erosion of fine sediment classes (fine sand, mud) due to the presence of coarser sediment particles within the mixture. Furthermore, this homogeneous treatment of sediment resuspension in the non-cohesive regime leads to more pronounced:

- residual horizontal fluxes of sand and mud, respectively 2 times and 30% larger than in the case of independent erosion of the sediment classes,
- ETM masses, on average 25% higher than in case of independent erosion over the simulated year,
- erosion/deposition patterns, especially over shoals (e.g., up to a two-fold erosion increase at the *Amfard* shoal), associated to specific seabed nature changes with bed sediment over areas subject to erosion generally coarser (or finer over areas subject to deposition) than in case of independent erosion.

The current study dedicated to the sediment dynamics of the Seine Estuary revealed more relevant erosion/deposition patterns (mainly resulting from fine to very fine sand dynamics) and a better representation of the average ETM mass when independent resuspension fluxes are considered in the non-cohesive regime (based on comparisons with observations). Therefore, results suggest that when sediment grain-size distributions become heterogeneous and multimodal regarding non-cohesive particles, an independent treatment of resuspension fluxes for each sediment class is more appropriate.

Bedload transport appears as a non-dominant but significant contributor to the sediment dynamics of the Seine Estuary (horizontal fluxes, erosion/deposition patterns, and seabed nature changes). Gradients of sediment flux (larger fluxes occurring over ebb delta shoals and in the main channel) and the resulting erosion/deposition patterns look generally similar between suspended load and bedload dynamics. Suspended sand fluxes generally dominate those caused by bedload, whatever the approach for modeling resuspension in the non-cohesive regime. On average, the residual bedload flux represents between 17 and 38% of the suspended sand flux, the lower contribution being obtained when suspended sediment fluxes result from homogeneous erosion in the non-cohesive regime. The bedload contribution to the total sediment transport increases when bed sediment becomes coarser (even dominant at specific locations), coarse sediment particles being hardly transported in suspension. Even though fluxes and bed level changes caused by bedload are, in general, spatially consistent with those associated with suspended load transport (especially of sand), the average orientation of the residual bedload fluxes can differ from the orientation related to suspended sediment fluxes over some areas like shoals, which results in particular erosion/deposition patterns. These specific erosion/deposition patterns linked to bedload are generally associated with a signature regarding the seabed nature. Sediment mass budgets cumulated over the simulated year reveal a relative contribution of bedload to total mass budgets around 25% over large erosion areas of shoals, which can even become higher in sedimentation zones.

Further research is required to assess more thoroughly the erosion flux formulation of muddy sediment in the non-cohesive regime. From the hydrodynamic point of view, accounting for specific 3D circulations induced by waves would constitute a

substantial improvement, which is likely to modulate morphological evolutions over near-shore shallow regions like shoals.

Declaration of competing interest

The authors declare that they have no known competing financial interests or personal relationships that could have appeared to influence the work reported in this paper.

Acknowledgments

The current study was done in the framework of the MORPHOSEINE project funded by the Seine-Aval 6 scientific research program. Tidal components from the CST France database are provided by the Service Hydrographique et Océanographique de la Marine (SHOM), river discharge data by the French freshwater office, and bathymetric data by the Groupe d'Intérêt Public (GIP) Seine Aval. The two anonymous reviewers are deeply thanked for their comments and suggestions that greatly improved the manuscript.

References

- Abbott, J. E., & Francis, J. R. D. (1977). Saltation and suspension trajectories of solid grains in a water stream. *Philosophical Transactions of the Royal Society of London - Series A: Mathematical and Physical Sciences*, 284(1321), 225–254.
- Bagnold, R. A. (1966). *An approach to the sediment transport problem from general physics*. U.S. Geological Survey. Professional Paper 422-D.
- Becherer, J., Hofstede, J., Gräwe, U., Purkiani, K., Schulz, E., & Burchard, H. (2018). The Wadden Sea in transition—consequences of sea level rise. *Ocean Dynamics*, 68(1), 131–151.
- Bi, Q., & Toorman, E. A. (2015). Mixed-sediment transport modelling in Scheldt estuary with a physics-based bottom friction law. *Ocean Dynamics*, 65(4), 555–587.
- Blanpain, O. (2009). *Dynamique sédimentaire multiclasse : de l'étude des processus à la modélisation en Manche* (Doctoral dissertation). University of Rouen, France. (In French)
- Carniello, L., Defina, A., & D'Alpaos, L. (2012). Modeling sand–mud transport induced by tidal currents and wind waves in shallow microtidal basins: Application to the Venice Lagoon (Italy). *Estuarine, Coastal Shelf Sci*, 102–103, 105–115.
- Craig, A., Valcke, S., & Coquart, L. (2017). Development and performance of a new version of the OASIS coupler, OASIS3-MCT_3.0. *Geoscientific Model Development*, 10(9), 3297–3308.
- Cuvilliez, A., Deloffre, J., Lafite, R., & Bessineton, C. (2009). Morphological responses of an estuarine intertidal mudflat to constructions since 1978 to 2005: The Seine estuary (France). *Geomorphology*, 104(3), 165–174.
- Deloffre, J., Lafite, R., Lesueur, P., Lesourd, S., Verney, R., & Guézennec, L. (2005). Sedimentary processes on an intertidal mudflat in the upper macrotidal Seine estuary, France. *Estuarine, Coastal Shelf Sci*, 64(4), 710–720.
- Deloffre, J., Lafite, R., Lesueur, P., Verney, R., Lesourd, S., Cuvilliez, A., & Taylor, J. (2006). Controlling factors of rhythmic sedimentation processes on an intertidal estuarine mudflat — role of the turbidity maximum in the macrotidal Seine estuary, France. *Marine Geology*, 235(1), 151–164.
- Demerliac, M. A. (1974). Calcul du niveau moyen journalier. *Annales Hydrographiques Du SHOM*, 5, 49–57. (In French)
- Dissanayake, D., Ranasinghe, R., & Roelvink, J. A. (2012). The morphological response of large tidal inlet/basin systems to relative sea level rise. *Climatic Change*, 113(2), 253–276.
- Dufois, F., & Le Hir, P. (2015). Formulating fine to medium sand erosion for suspended sediment transport models. *Journal of Marine Science and Engineering*, 3, 906–934.
- Dufois, F., Verney, R., Le Hir, P., Dumas, F., & Charmasson, S. (2014). Impact of winter storms on sediment erosion in the Rhone river prodelta and fate of sediment in the Gulf of Lions (north western mediterranean sea). *Continental Shelf Research*, 72, 57–72.
- Durafour, M., Jarno, A., Le Bot, S., Lafite, R., & Marin, F. (2015). Bedload transport for heterogeneous sediments. *Environmental Fluid Mechanics*, 15(4), 731–751.
- Franz, G., Leitão, P., Pinto, L., Jauch, E., Fernandes, L., & Neves, R. (2017). Development and validation of a morphological model for multiple sediment classes. *International Journal of Sediment Research*, 32(4), 585–596.
- Grasso, F., & Le Hir, P. (2019). Influence of morphological changes on suspended sediment dynamics in a macrotidal estuary: Diachronic analysis in the Seine Estuary (France) from 1960 to 2010. *Ocean Dynamics*, 69(1), 83–100.
- Grasso, F., Le Hir, P., & Bassoullet, P. (2015). Numerical modelling of mixed-sediment consolidation. *Ocean Dynamics*, 65(4), 607–616.
- Grasso, F., Verney, R., Le Hir, P., Thouvenin, B., Schulz, E., Kervella, Y., ... Garnier, V. (2018). Suspended sediment dynamics in the macrotidal Seine Estuary (France):

- 1
2
3
4
5
6
7
8
9
10
11
12
13
14
15
16
17
18
19
20
21
22
23
24
25
26
27
28
29
30
31
32
33
34
35
36
37
38
39
40
41
42
43
44
45
46
- Q4
1. Numerical modeling of turbidity maximum dynamics. *Journal of Geophysical Research: Oceans*, 123(1), 558–577.
- Guérin, T., Bertin, X., & Chaumillon, E. (2016). Wave control on the rhythmic development of a wide estuary mouth sandbank: A process-based modelling study. *Marine Geology*, 380, 79–89.
- Guérin, T., Bertin, X., Coulombier, T., & de Bakker, A. (2018). Impacts of wave-induced circulation in the surf zone on wave setup. *Ocean Modelling*, 123, 86–97.
- Harris, C. K., & Wiberg, P. L. (1997). Approaches to quantifying long-term continental shelf sediment transport with an example from the Northern California STRESS mid-shelf site. *Continental Shelf Research*, 17(11), 1389–1418.
- Jacobsen, N. G., & Fredsoe, J. (2014). Formation and development of a breaker bar under regular waves. Part 2: Sediment transport and morphology. *Coastal Engineering*, 88, 55–68.
- Jonsson, I. G. (1966). Wave boundary layers and friction factors. *Coastal Eng Proc*, 1(10), 9.
- Krone, R. B. (1962). *Flume studies of the transport of sediment in estuarine shoaling processes. Final report to San Francisco district*. Washington, DC: U.S. Army Corps of Engineers.
- Lazure, P., & Dumas, F. (2008). An external–internal mode coupling for a 3D hydrodynamical model for applications at regional scale (MARS). *Advances in Water Resources*, 31(2), 233–250.
- Le Hir, P., Cayocca, F., & Waeles, B. (2011). Dynamics of sand and mud mixtures: A multiprocess-based modelling strategy. *Continental Shelf Research*, 31(10, Supplement), S135–S149.
- van Ledden, M. (2003). *Sand-mud segregation in estuaries and tidal basins* (Doctoral dissertation). Delft University.
- van Ledden, M., Wang, Z.-B., Winterwerp, H., & de Vriend, H. (2004). Sand–mud morphodynamics in a short tidal basin. *Ocean Dynamics*, 54(3), 385–391.
- Lemoine, J.-P., Le Hir, P., & Grasso, F. (2017). Impacts of maintenance dredging on suspended sediment dynamics in the Seine estuary. In F. Pedocchi, S. Vinzon, & C. Friedrichs (Eds.), *Proceedings, 14th international conference on cohesive sediment transport processes (INTERCOH)*, (pp. 110–111), Montevideo, Uruguay.
- Lesourd, S., Lesueur, P., Brun-Cottan, J.-C., Auffret, J.-P., Poupinet, N., & Laignel, B. (2001). Morphosedimentary evolution of the macrotidal Seine estuary subjected to human impact. *Estuaries*, 24(6), 940.
- Lesourd, S., Lesueur, P., Fisson, C., & Dauvin, J.-C. (2016). Sediment evolution in the mouth of the seine estuary (France): A long-term monitoring during the last 150 years. *Comptes Rendus Geoscience*, 348(6), 442–450.
- Lesser, G. R., Roelvink, J. A., van Kester, J. A. T. M., & Stelling, G. S. (2004). Development and validation of a three-dimensional morphological model. *Coastal Engineering*, 51(8), 883–915.
- Mengual, B., Le Hir, P., Cayocca, F., & Garlan, T. (2017). Modelling fine sediment dynamics: Towards a common erosion law for fine sand, mud and mixtures. *Water*, 9(8), 564.
- Meyer-Peter, E., & Müller, R. (1948). Formulas for bed-load transport. In *Proceedings, 2nd meeting of the international association for hydraulic structures research* (pp. 39–64), Stockholm.
- Mitchener, H., & Torfs, H. (1996). Erosion of mud/sand mixtures. *Coastal Engineering*, 29(1–2), 1–25.
- Partheniades, E. (1965). Erosion and deposition of cohesive soils. *Journal of the Hydraulics Division*, 91, 105–139.
- Reniers, A., Gallagher, E. L., MacMahan, J. H., Brown, J. A., van Rooijen, A. A., van Thiel de Vries, J. S. M., & van Prooijen, B. C. (2013). Observations and modeling of steep-beach grain-size variability. *Journal of Geophysical Research: Oceans*, 118(2), 577–591.
- van Rijn, L. C. (1989). *Handbook sediment transport by currents and waves*. Delft, The Netherlands: Delft Hydraulics Laboratory.
- van Rijn, L. C. (2007). Unified view of sediment transport by currents and waves. I: Initiation of motion, bed roughness, and bed-load transport. *Journal of Hydraulic Engineering*, 133(6), 649–667.
- van Rijn, L. C., Ribberink, J. S., Werf, J. V. D., & Walstra, D. J. R. (2013). Coastal sediment dynamics: Recent advances and future research needs. *Journal of Hydraulic Research*, 51(5), 475–493.
- Rivier, A., Le Hir, P., Bailly du Bois, P., Laguionie, P., & Morillon, M. (2017). Numerical modelling of heterogeneous sediment transport: New insights for particulate radionuclide transport and deposition. In T. Aagaard, R. Deigaard, & D. Fuhrman (Eds.), *Proceedings, coastal dynamics 2017* (pp. 1767–1778). Denmark: Helsingør.
- Rodi, W. (1993). *Turbulence models and their application in hydraulics* (3rd ed.). Delft, The Netherlands: IAHR Monograph.
- Roland, A., & Arduin, F. (2014). On the developments of spectral wave models: Numerics and parameterizations for the coastal ocean. *Ocean Dynamics*, 64(6), 833–846.
- Schulz, E., Grasso, F., Le Hir, P., Verney, R., & Thouvenin, B. (2018). Suspended sediment dynamics in the macrotidal seine Estuary (France): 2. Numerical modeling of sediment fluxes and budgets under typical hydrological and meteorological conditions. *Journal of Geophysical Research: Oceans*, 123(1), 578–600.
- Seity, Y., Brousseau, P., Malardel, S., Hello, G., be Nard, P., Bouttier, F., Lac, C., & Masson, V. (2011). The AROME-France convective-scale operational model. *Monthly Weather Review*, 139(3), 976–991.
- Soulsby, R. (1997). *Dynamics of marine sands: A manual for practical applications*. London: Thomas Telford Ltd.
- Soulsby, R. L., & Damgaard, J. S. (2005). Bedload sediment transport in coastal waters. *Coastal Engineering*, 52(8), 673–689.
- Soulsby, R. L., Hamm, L., Klopman, G., Myrhaug, D., Simons, R. R., & Thomas, G. P. (1993). Wave-current interaction within and outside the bottom boundary layer. *Coastal Engineering*, 21(1), 41–69.
- Waeles, B. (2005). *Modélisation morphodynamique de l'embouchure de la Seine* (Doctoral dissertation). University of Caen, France. (In French)
- Waeles, B., Le Hir, P., Lesueur, P., & Delsinne, N. (2007). Modelling sand/mud transport and morphodynamics in the Seine River mouth (France): An attempt using a process-based approach. *Hydrobiologia*, 588(1), 69–82.
- Waeles, B., Le Hir, P., & Lesueur, P. (2008). A 3D morphodynamic process-based modelling of a mixed sand/mud coastal environment: The Seine Estuary, France. *Proceedings in Marine Science*, 9, 477–498.
- Warner, J. C., Sherwood, C. R., Signell, R. P., Harris, C. K., & Arango, H. G. (2008). Development of a three-dimensional, regional, coupled wave, current, and sediment-transport model. *Computers & Geosciences*, 34(10), 1284–1306.
- Introduction to the physics of cohesive sediment dynamics in the marine environment. In Winterwerp, J. C., & van Kesteren, W. G. (Eds.), *Developments in sedimentology* (Vol. 56), (2004). Amsterdam: Elsevier.
- Wu, W., & Lin, Q. (2014). Nonuniform sediment transport under non-breaking waves and currents. *Coastal Engineering*, 90, 1–11.
- Wu, W., Wang, S. S., & Jia, Y. (2000). Nonuniform sediment transport in alluvial rivers. *Journal of Hydraulic Research*, 38(6), 427–434.
- van der Zanden, J., van der A. D. A., Hurther, D., Cáceres, I., O'Donoghue, T., Hulscher, S. J. M. H., & Ribberink, J. S. (2017). Bedload and suspended load contributions to breaker bar morphodynamics. *Coastal Engineering*, 129, 74–92.
- Zheng, P., Li, M., van der A. D. A., van der Zanden, J., Wolf, J., Chen, X., & Wang, C. (2017). A 3D unstructured grid nearshore hydrodynamic model based on the vortex force formalism. *Ocean Modelling*, 116, 48–69.
- 47
48
49
50
51
52
53
54
55
56
57
58
59
60
61
62
63
64
65
66
67
68
69
70
71
72
73
74
75
76
77
78
79
80
81
82
83
84
85
86
87
88
89
90
91
92